Tropical cloud forest climate variability and the demise of the Monteverde golden toad

Kevin J. Anchukaitis[a,b,1] and Michael N. Evans[a,b,c]

[a]Lamont-Doherty Earth Observatory of Columbia University, Palisades, NY 10964; [b]Laboratory of Tree-Ring Research, University of Arizona, Tucson, AZ 85721; and [c]Department of Geology & Earth System Science Interdisciplinary Center, University of Maryland, College Park, MD 20740

Edited by Lisa Graumlich, University of Arizona, Tucson, AZ, and accepted by the Editorial Board February 1, 2010 (received for review July 29, 2009)

Widespread amphibian extinctions in the mountains of the American tropics have been blamed on the interaction of anthropogenic climate change and a lethal pathogen. However, limited meteorological records make it difficult to conclude whether current climate conditions at these sites are actually exceptional in the context of natural variability. We use stable oxygen isotope measurements from trees without annual rings to reconstruct a century of hydroclimatology in the Monteverde Cloud Forest of Costa Rica. High-resolution measurements reveal coherent isotope cycles that provide annual chronological control and paleoclimate information. Climate variability is dominated by interannual variance in dry season moisture associated with El Niño Southern Oscillation events. There is no evidence of a trend associated with global warming. Rather, the extinction of the Monteverde golden toad (*Bufo periglenes*) appears to have coincided with an exceptionally dry interval caused by the 1986–1987 El Niño event.

Costa Rica | ENSO | extinction | stable isotopes

The demise of the Monteverde golden toad (*Bufo periglenes*) in the montane cloud forest of Costa Rica in 1987–1988, as well as subsequent amphibian extinctions throughout the American tropics, has been believed to be a consequence of the interaction of global warming (1, 2) and the introduced chytrid fungus *Batrachochytrium dendrobatidis* (3–5). Analysis of the limited available weather data from Monteverde has suggested that a trend toward decreasing immersion cover since the late 1970s reflects the influence of increasing tropical air and sea surface temperatures (SST) (1, 2). Pounds and coauthors (1) argued that this pattern of increasing dry days implicated rising global temperatures due to anthropogenic greenhouse gas emissions. Nair et al. (6) and Lawton et al. (7) used a regional atmospheric model to demonstrate that deforestation in the tropical lowland forests upwind from the Monteverde Cloud Forest could also potentially result in elevated cloud base height and drier conditions.

Subsequent examination of a larger dataset of the last year of observation (LYO) of extinct neotropical amphibians in the genus *Atelopus* found a positive, lagged correlation between mean annual tropical (30 °N to 30 °S) temperatures and the timing of *Atelopus* extinctions (2). The authors hypothesized that temperatures at many montane locations in the Americas were shifting towards an "optimum range" for the growth of the chytrid fungus. This "chytrid-thermal-optimum hypothesis" suggested that tropical temperature trends associated with anthropogenic global warming were responsible for widespread amphibian extinctions due to chytridiomycosis.

This "climate-linked epidemic hypothesis" (2) postulates that global warming contributes to the development of optimal environmental conditions for the fungus. Upward trends in global temperatures could therefore already be fundamentally altering the suite of climatic conditions that maintain mountain forest ecosystems in Central America. General circulation model simulations of climate under doubled CO_2 conditions predict higher lifting condensation levels and reduced cloud contact for tropical montane cloud forests as a result of increasing temperatures (8). Imprinted on the apparent instrumental drying trend at Monteverde, El Niño events also cause local increases in temperature and reductions in cloud cover and moisture (9). However, the role of climate change in neotropical anuran extinctions has been questioned on statistical grounds (10, 11). Without the context provided by long-term climate records, it is difficult to confidently conclude whether the extinction of the golden toad and other changes in cloud forest ecology are the consequence of anthropogenic climate forcing (2), land-surface feedbacks due to deforestation (6, 7), or natural variability in tropical climate (9).

Approach

We developed annual proxy records of climate variability from tropical montane cloud forest trees without annual rings at Monteverde (10.2 °N, 85.35 °W, 1500–1800 m) over the last century using stable isotopes (12, 13). The advantage of this approach is that it does not rely on the formation of yearly morphological growth hiatuses in trees, which in the tropics can often be absent (Fig. 1*A*), but rather takes advantage of the annual variation in the stable oxygen isotope ratio ($\delta^{18}O$) of water used by plants over the course of a year. This technique can also be applied where posited "growth rings" cannot be shown to be annual. Annual oxygen isotope cycles have been identified in lowland tropical forests (12, 14), and at Monteverde we have previously demonstrated that variation between the summer wet season and the cloud-dominated winter dry season is sufficient to induce an annual $\delta^{18}O$ cycle along the radial xylem growth of cloud forest trees (13). The $\delta^{18}O$ of cellulose in cloud forest trees reflects the seasonal change in the $\delta^{18}O$ of source water as determined by the amount of rainfall and the ^{18}O-enrichment of cloud water. On interannual time scales, departures from the mean annual cycle amplitude will result from anomalous rainfall and changes in temperature, relative humidity, and evapotranspiration (13, 15). At Monteverde, these are further related to changes in the intensity of moisture advection over the continental divide into the Pacific slope forests and the amount of cloud cover. Interannual changes in the annual $\delta^{18}O$ cycle maxima can therefore be interpreted as moisture changes during the boreal winter dry season (approximately January to April).

We made high-resolution (200 μm increment) stable oxygen isotope ratio measurements along the radial growth axis of two *Pouteria*, mature canopy trees in the Sapotaceae family growing in the cloud forest on the Pacific slope below the continental divide at Monteverde, using a unique online induction pyrolysis system (16). The resulting $\delta^{18}O$ data series have coherent annual oxygen isotope cycles we use for chronological control (Fig. 1 *B* and *C*) in the absence of rings. We developed an age model for both series by assigning the maxima of each discrete cycle to the

Author contributions: K.J.A. designed research; K.J.A. performed research; M.N.E. contributed new reagents/analytic tools; K.J.A. and M.N.E. analyzed data; and K.J.A. and M.N.E. wrote the paper.

The authors declare no conflict of interest.

This article is a PNAS Direct Submission. L.G. is a guest editor invited by the Editorial Board.

[1]To whom correspondence should be addressed. E-mail: kja@ldeo.columbia.edu.

This article contains supporting information online at www.pnas.org/cgi/content/full/0908572107/DCSupplemental.

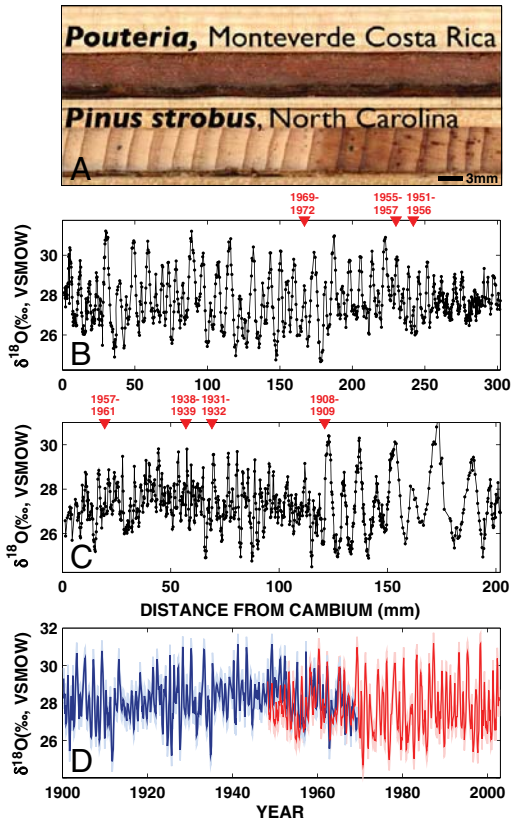

Fig. 1. Oxygen isotope cycles in *Pouteria* at Monteverde. (*A*) Unlike most temperate region trees (for example, the *Pinus strobus* from North Carolina shown here), *Pouteria* from Monteverde lack any identifiable annual rings. However, stable oxygen isotope measurements on two *Pouteria* trees reveal consistent annual cycles in the δ^{18}O data sampled at constant increments from the cambium in samples MV12 (*B*) and MV15 (*C*). Seven radiocarbon dates are shown by red triangles. Further ^{14}C calibration details are available in *SI Text*. Note that the two cores do not span the same exact time period (see *Mathods and Materials*). (*D*) Monthly age modeled δ^{18}O series from MV12 (red) and MV15 (blue) as a function of time, with lighter colors showing $\pm 2\sigma$ analytical error.

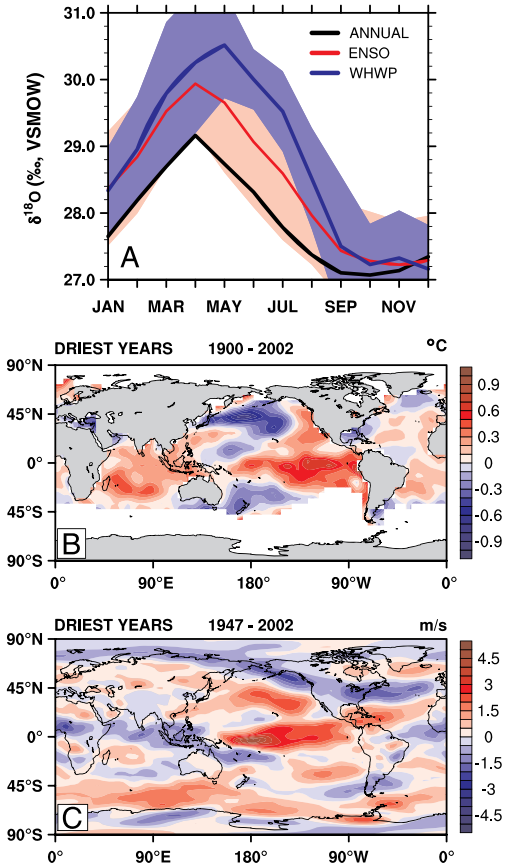

Fig. 2. Association between Monteverde δ^{18}O records and regional/global climate. (*A*) Annual δ^{18}O cycles are clearly enriched during warm ENSO events (red line; 1905, 1926, 1942, 1952, 1958, 1966, 1969, 1978, 1983, 1987, 1992, and 1998) and extensive WHWP (blue line; 1958, 1969, 1987, 1998) years (20) (*A*), relative to the overall mean (black line). $\pm 1\sigma$ confidence intervals are shown by same-color shading. (*B*) The 10 most enriched years in the isotope chronology are associated with an average dry season (January-April) SST anomaly (18) in the eastern Pacific of greater than 1 °C. (*C*) Similarly, positive dry season (January-April) δ^{18}O anomalies are associated with weaker 850 mb tradewinds in both the tropical Atlantic and Pacific (19).

dry season of the corresponding year and interpolating the δ^{18}O data series between these tie points to monthly resolution (13) Fig. 1(*D*). Radiocarbon assays confirm our age modeled δ^{18}O time series, which spans the period 1900 to 2002, with an estimated overall age model error of ± 2 years (details of the radiocarbon analysis are available as *SI Text*).

Results

Annual δ^{18}O cycles show a mean amplitude of 2.16‰ (Fig. 1 *B–D*; Fig. 2*A*), with an average magnitude of year-to-year variability of 50% of this annual cycle ($\sigma = 1.08$‰). We observe significant correlations consistent with pilot studies and the interpretive hypothesis for annual and interannual variability described above. Collectively, dry and wet season temperature and precipitation, dry season zonal wind speed, and dry season relative humidity explain 40% of the annual cycle amplitude variability in our δ^{18}O time series over the instrumental period at Monteverde. These empirical correlations are also consistent with expectations from independent, mechanistic modeling (15, 17) of expected cellulose δ^{18}O as a function of climate (Fig. S1 and *SI Text*). Dry season amplitude anomalies also show a clear relationship to interannual climate variability in sea surface temperature anomalies (18) and zonal wind velocity (19) (Fig. 2 *B* and *C*). El Niño Southern Oscillation (ENSO) years in the δ^{18}O chronology show a isotopic cycle enrichment 0.8‰ (greater than 1σ) above the mean (Fig. 2*A*), with a strong mean positive anomaly of 2.0‰ for 1983, 1987, and 1998 alone (greater than 2σ above the mean). These years of discernible strong positive anomalies in the monthly δ^{18}O chronology (Fig. 3*A*) correspond to periods of dry season drought (greater number of consecutive dry days), negative dry season precipitation anomalies, and temperature anomalies of a degree Celsius or more (1). ENSO years have significantly higher δ^{18}O values in the dry and early wet season (January through July, one-tailed paired *t* test, $p < 0.01$). In addition to dry season variability associated with these strong El Niño events, there are larger mean positive δ^{18}O anomalies of ~1.8‰ in years of substantially warmer tropical Atlantic and Western Hemisphere warm pool (WHWP) temperatures (20). The anomalous peak (greater than 2σ above the mean) δ^{18}O associated with warm WHWP events indicates a later onset of the rainy season and the effective moisture deficit persists for several months. The end of the dry season and early wet season (May through July) are significantly higher when WHWP events ($n = 4$) are considered alone (one-tailed paired *t* test, $p < 0.01$), consistent with the association of the largest magnitude WHWP warm events with El Niño events that have persistent boreal spring SST anomalies (20).

A weakening of local and equatorial Pacific 850 mb (~1,500 m) easterly winds appears to consistently accompany the δ^{18}O anomalies over the length of the reanalysis period (19) (Fig. 2*C*). Those years with anomalously high maximum δ^{18}O values occur simultaneously with dry season westerly zonal

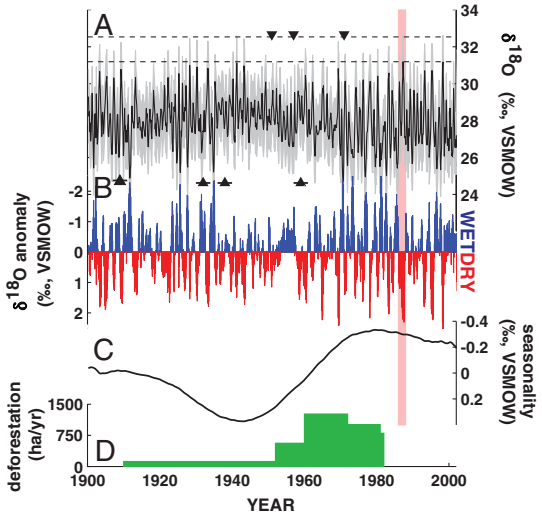

Fig. 3. Composite isotope time series and inferred moisture anomalies at Monteverde. (*A*) The composite monthly δ^{18}O time series shows coherent annual isotope cycles back to 1900. The composite series was developed by averaging the two δ^{18}O series after first dilating the variance of MV15 to that of MV12 as estimated over their common 253 month overlap. Differences in the long-term mean and common period variance of the two series are only slightly higher (0.35 and 0.41‰) than analytical precision (0.28‰). Gray shading indicates the full envelope of additive uncertainty due to analytical measurement precision and the observed differences in variance and mean between the overlapping section of the cores. Since these three different elements of total uncertainty are not independent, this envelope is likely conservative. δ^{18}O enrichment associated with the 1986–1987 ENSO/WHWP event is highlighted, with horizontal dashed lines in (*A*) indicating the most likely range of dry season isotopic maxima for 1987, given uncertainties. Radiocarbon dates and their uncertainty are shown by filled triangles and their associated horizontal bars. (*B*) Monthly δ^{18}O anomalies from the mean annual cycle emphasize that the time period associated with the 1986–1987 warm ENSO event was one of the driest of the last century. (*C*) Multidecadal variability in δ^{18}O (SSA filtered, $M = 20$ years) shows changes in the magnitude of δ^{18}O seasonality. (*D*) Deforestation rates in Costa Rica's Atlantic forests upwind from Monteverde (30).

wind anomalies. Because the slackening of the northeasterly tradewinds at Monteverde will influence moisture advection over the continental divide, the relationship between the dry season amplitude and local zonal wind anomalies from reanalysis data also accounts for the largest portion of the total variance in δ^{18}O amplitude of any single local climate variable ($r = 0.53$, $p = 0.01$) (Fig. 2*C*). Higher temperature and lower relative humidity display similar associations with the isotope chronology and likewise covary with ENSO and WHWP events. Anomalous δ^{18}O peaks that occur during warm ENSO and WHWP events coincide with increased Monteverde temperature, weaker zonal winds, and reduced relative humidity and precipitation; however, smaller δ^{18}O dry season anomalies can also occur in ENSO neutral years when only one or two of these climatic factors is anomalous.

A distinct change in the amplitude of the annual δ^{18}O cycle occurs in the middle or late 1960s (Fig. 1*D*; Fig. 3 *A* and *C*) and is related to a change in both the wet season minima and the dry season amplitude, suggesting an overall damped seasonality, reduced summer rainfall, and slightly increased dry season moisture for the period from the mid-1930s through the 1960s. There is support for this interpretation from the limited climate station data from the Pacific side of northwestern Costa Rica that spans the period of the transition, which shows an increase in precipitation between 1960 and 1970 (21, 22). The previous Monteverde station, downslope from the cloud forest (1,460 m elevation), shows an increase in average summer precipitation of approximately 200 mm over the 1960s, which could translate into a change in the δ^{18}O of rainy season precipitation of as much as ~1.2‰ (13, 23), approximately the same as observed in our isotope chronology. However, the association between the δ^{18}O time series amplitude and the concurrent zonal wind field retains its spatial pattern and magnitude, reinforcing our interpretation that the most consistent and proximal control on dry season moisture at Monteverde is the strength of the easterly winds. The change to high amplitude δ^{18}O cycles in the late 1960s coincides with a shift in the sign of the summer North Atlantic Oscillation (NAO) index (24), an increase in interannual band (ENSO) variance in the tropical Pacific (25–27), a change in the seasonality of ENSO (28), and with other rapid changes in patterns of global atmosphere circulation, particularly in the tropical and Atlantic regions (24). Positive phases of the NAO, such as observed after the 1960s, are associated with positive precipitation anomalies in the early wet season in Central America (29). At the same time, deforestation rates in the Atlantic coast forests of Costa Rica increased (Fig. 3*D*) (30) and could have contributed to mesoscale alterations of boundary layer interactions sufficient to influence downwind dry season cloud formation (6, 7).

We empirically identify temporal patterns in our δ^{18}O time series using singular spectrum analysis (SSA) (31–33). The identification of interpreted spectral components is robust to the choice of embedding dimension. Leading modes contain annual and 2–6 yr periodicities and explain 34% and 12% of total monthly signal variance, respectively. ENSO band frequencies contain 34% of the power at annual resolution. Only one significant low order eigenvector is dominated by multidecadal variance, with a prominent spectral peak between 20 and 30 yr (Fig. 3*C*). This reflects changes in the annual isotope amplitude, or seasonality, since we determined that removing the annual cycle prior to SSA causes this component to disappear entirely. A monthly anomaly series (Fig. 3*B*) is recovered by calculating the difference between each monthly δ^{18}O value and the overall mean ($n = 102$) δ^{18}O "climatology" for the corresponding month.

Discussion

Causes of the Demise of the Monteverde Golden Toad. The early study of the relationship between the hydroclimatology of Monteverde and ENSO events by Pounds and Crump (9) noted the strong drying which occurred during the 1986–1987 El Niño event and identified higher temperatures and lower seasonal rainfall as well during the prior (1982–1983) El Niño. In that case, warmer Pacific SSTs were interpreted to correspond to warmer, drier conditions in the cloud forest. Based on statistical hypothesis testing, Pounds and coauthors (34) subsequently concluded that the abnormal dry conditions of 1987 were likely to have caused the multispecies population crash, which included the extinction of the Monteverde Golden Toad. Both of these papers speculated at the time that disease may have been the proximate cause of the extinction of the golden toad (9, 34). Chytridiomycosis, caused by the chytrid fungus *Batrachochytrium dendrobatidis*, was eventually identified as a major cause of amphibian extinction throughout the Americas, Europe, Australia, and New Zealand (3–5).

The "chytrid-thermal-optimum hypothesis" suggested that tropical temperature trends associated with anthropogenic global warming were responsible for widespread amphibian extinctions due to chytridiomycosis (2), and the earlier work (1) associated the extinction of the golden toad with dry conditions at Monteverde. Lips et al. (11) tested the robustness of the statistical comparison between tropical temperatures and *Atelopus* LYO data, concluding that uncertainties in the choice of anuran observational data were sufficient to call into question the relationship. These authors instead sought to demonstrate that spatial patterns of extinction due to chytridiomycosis could be related to the spread of the fungus from a few centers of initial infection. Rohr et al (2008) (10) questioned both conclusions and stated that "Almost all of our findings are contrary to the predictions of the 'chytrid-thermal-optimum hypothesis.' " They also found that

there was no stable linear relationship between the diurnal temperature range and modeled growth of the chytrid fungus. Significant correlations were found, however, between modeled chytrid fungus mortality and decreases in cloud cover (10).

The significant drying trend in the number of days without rainfall identified by Pounds and coauthors (1, 2) is a result of the rapid increase in the number of annual dry days beginning with the strong 1982–1983 El Niño and the occurrence of long periods of drought during the 1998 dry season, also associated with ENSO. This trend is sensitive to the range of years and the threshold of consecutive days utilized (see Fig. S2 and *SI Text*). We have also determined that, due to the limited length of the record, there is no statistically significant difference [$p \geq 0.26$ (35)] in the correlation between the LYO for *Atelopus* and annual tropical temperatures ($r = 0.76$, $p = 0.001$), the Atlantic Multidecadal Oscillation index ($r = 0.54$, $p = 0.04$) (18, 36), or average spring-summer sea surface temperatures in the WHWP ($r = 0.48$, $p = 0.06$) (20).

Contrary to interpretations of the short instrumental record (1), no long-term trend in dry season hydroclimatology can be inferred from our δ^{18}O time series at Monteverde (1900–2002, $p = 0.50$; 1973–2000, $p = 0.31$). Rather, variability at the interannual scale dominates the isotope signal, particularly during the period of increased ENSO variance since the late 1960s. The years 1983, 1987, and 1998 are the three driest winters in the last three decades (Fig. 3*A*). Collectively, the period from 1986 to 1988, associated with a strong El Niño event and an extensive WHWP that persisted into boreal late spring-summer, appears to be one of the driest in the last three decades and is amongst the driest of the last century (Fig. 3*B*). The strong warm ENSO event of 1997–1998 was also followed by demographic shifts in anuran populations at Monteverde (1). There is currently no consensus on how anthropogenic climate change will influence the El Niño Southern Oscillation (37, 38) and ENSO anomalies in the most recent decades are not beyond the range of natural variability during the instrumental period (39). This suggests that the cause of the specific and well-documented extinction of the Monteverde golden toad was the combination of the abnormally strong ENSO-forced dryness (9) and the lethality (3) of the introduced chytrid fungus, but was not directly mediated by anthropogenic temperature trends, a finding from paleoclimatology that is in agreement with statistical reanalysis (10, 11) of the "climate-linked epidemic hypothesis."

In light of these results, the early hypotheses by Pounds and coauthors about the potential role of warm ENSO events in driving recent ecological change at Monteverde now appear prescient (9, 34). Our δ^{18}O chronology from Monteverde allows us to conclude that one of the longest driest periods in the last 100 yr occurred during the 1986–1987 El Niño. It is possible that *Batrachochytrium dendrobatidis* was already present in Monteverde prior to that year (40). Dry conditions culminating during the reproductive season in 1987 would have caused amphibian populations to coalesce around a few remaining wet microhabitats (1, 34, 41), where the fungus would have been able to spread rapidly through the population and ultimately result in extinction.

Sources of Uncertainty. While high-resolution oxygen isotope measurements allow us to resolve the annual cycle of source water δ^{18}O and isotopic enrichment in cloud forest trees, and to therefore establish chronological control even in the absence of annual rings, there are a number of uncertainties that necessitate cautious interpretation of the chronological and climatic information in our δ^{18}O time series. Our approach to developing records of past climate from tropical trees (12) has a closer methodological and procedural affinity to paleoclimate analysis using speleothems or corals than to classical dendrochronology. Although chronological uncertainty in this study is minimized through the combination of the identification of annual stable isotope cycles (13) and radiometric dating, we do not achieve the age model precision available from traditional approaches to dendrochronology that use large sample sizes and robust statistical pattern matching (42), nor can we be certain we have identified "missing" years. While the δ^{18}O signal of cellulose from tree rings will be dominated by the enrichment due to transpiration and the source water signal associated with the amount effect (43), the latter accounts for only a portion of the total variability in precipitation δ^{18}O (13) and the former could be influenced by several additional environmental and physiological factors; only the effects of precipitation, temperature, humidity, and wind are accounted for directly in our analysis. We have found that the observed annual and interannual δ^{18}O variability in our *Pouteria* trees match those expected from both our hypothesis and mechanistic simulations. However, additional replication is necessary to place more confidence in estimates of multidecadal variability.

On the Role of Climate and Disease in Extinction Events. Epidemic-driven extinction may be the result of a series of biotic and abiotic interactions across spatial and temporal scales (11, 44). Drought or pluvial conditions associated with strong ENSO events are known to be associated with localized extinction (45, 46). In Yellowstone National Park, amphibian declines have been linked to the combination of decreasing precipitation, increasing temperatures, and wetland desiccation, which affects populations by contributing to increasing mortality, decreased migration, and reduced opportunities for wetland colonization (47). The decline of amphibians in El Yunque Forest in Puerto Rico is believed to be a consequence of a change in their behavior during dry periods, with populations moving from a dispersed distribution to a few protected microsites on the landscape, increasing their vulnerability to contagion (48). Similar patterns were observed at Monteverde prior to the multispecies population crash and extinction of the golden toad in 1987 (1, 9, 34, 41). Extinction events are an omnipresent feature of the history of life (49). Hence, while climate anomalies are not a feature of all extinctions (11, 44), it is not unreasonable to expect that natural climate variability can interact with species life history and ecological community and population dynamics to contribute to extinctions, even as anthropogenic climate change continues to develop. Indeed, future increases in tropical temperatures, in conjunction with interannual or decadal variability, may exacerbate stresses on tropical montane ecosystems.

Materials and Methods

Stable Oxygen Isotopes. Increment cores from two individual mature Sapotaceae (*Pouteria*) were collected at an elevation of 1,560 (MV12) and 1,580 m (MV15). MV12 was struck by lightning and subsequently felled in 2002. Radiocarbon measurements on MV15 revealed that it had an outer wood date more recent than 1960. The cores were subsampled in the laboratory at continuous 200 μm increments using a rotary microtome. The raw wood samples were chemically processed to α-cellulose using the Brendel method (50, 51) as modified for high-resolution sampling (12), and 300–350 μg of α-cellulose were wrapped in silver capsules and converted online to CO in a Costech High Temperature Generator/Elemental Combustion System (HTG/ECS) (16). At the time these analyses were conducted, this was the minimum sample size necessary to achieve acceptable measurement precision, and therefore determined the sampling increment on the 5 mm diameter cores collected from our *Pouteria* trees from Monteverde. The HTG uses a 1 MHz radio frequency induction heater to rapidly raise the temperature of a thin molybdenum crucible susceptor packed with graphite to >1, 500 °C for highly efficient pyrolysis (16). Isotopic measurements were made using a Costech induction heater coupled to a ThermoFinnigan Delta XP continuous flow isotope ratio mass spectrometer (16). Measurement precision on a total of 320 interspersed Sigma Alpha Cellulose solid standards was 0.28‰.

Radiocarbon and Chronology Validation. Seven samples from the two cores were selected for radiocarbon analysis to test the δ^{18}O-based age model. We estimate that maximum age model error for the earliest part of our chronology to be ±1 yr, based on the range of realistic age models as constrained by the 2σ resolution of the post-1955 radiocarbon dates. The older (1900–1949) portion of the chronology has an estimated maximum

age model error of ±2 yr due to slower growth rates and lower radiocarbon precision. The actual calendar dates that could be realistically associated with the radiocarbon assays, particularly on MV15, can be better constrained using Bayesian probability estimates between the radiocarbon calibration curve and the sample measurements (52–54). The likely dates are restricted foremost by the growth orientation of the tree—that is, samples from near the bark must be more recently formed than those near the center of tree—and secondly using the number of annual cycles between each $\Delta^{14}C$ measurement, in order to determine the most probable interval spanned by the core. One radiocarbon age from MV15 is post-bomb (AA776775) and provides an anchor for constraining the remaining three prebomb dates. Within these temporal, self-consistent constraints, the radiocarbon measurements and their individual probability density functions are then matched against the calibration curve and a posteriori probability functions calculated. Applying Bayesian analysis and these additional restrictions reveals that the core from MV15 spans the period 1900–1969 (Table S1). As an independent check on chronology development from both cycle counting and radiocarbon dating, we cross-correlated the "floating" MV15 sequence with the securely dated MV12 chronology. Even without additional age control constraints from $\Delta^{14}C$, a span of 1900–1969 for MV15 has the largest cross-correlation with MV12 for the monthly $\delta^{18}O$ values [$r = 0.43$, $p = 0.016$, (55)], the monthly mean ($r = 0.44$, $p < 0.01$), and the monthly minimum ($r = 0.65$, $p < 0.01$) $\delta^{18}O$, which mirrors the independent high-resolution radiocarbon dating described above.

ACKNOWLEDGMENTS. Todd Lange was instrumental in securing radiocarbon dates. We are grateful for comments and suggestions from Julio Betancourt, Malcolm Hughes, Mary Gagen, Julie Cole, Jonathan Overpeck, and Tim Shanahan. We benefitted tremendously from excellent laboratory and field assistance from John Buchanan, Mau-Chuang Foo, Lisa Wade, Frank Joyce, Alan Pounds, Rex Adams, Jim Burns, Sarah White, Arturo Cruz, Eladio Cruz, and Koky Porras. We thank the Organization for Tropical Studies for help with permits and Alan Pounds and the Tropical Science Center for access to the Monteverde Cloud Forest Reserve (Rafael Bolaños and Carlos Hernandez) and surrounding areas. We thank two anonymous reviewers for critiques that helped improve the manuscript. This research was supported by a graduate training fellowship from the National Science Foundation (NSF) IGERT Program (DGE-0221594) (to K.J.A.), a Graduate Research Environmental Fellowship (to K.J.A.) from the U.S. Department of Energy, and NSF Grants ATM-0349356 and ATM-0321348 (to M.N.E.). Data are available from the NOAA World Data Center for Paleoclimatology (http://www.ncdc.noaa.gov/paleo/paleo.html). This is LDEO Contribution #7326.

1. Pounds JA, Fogden M, Campbell JH (1999) Biological response to climate change on a tropical mountain. *Nature* 398:611–615.
2. Pounds JA, et al. (2006) Widespread amphibian extinctions from epidemic disease driven by global warming. *Nature* 439:161–167.
3. Berger L, et al. (1998) Chytridiomycosis causes amphibian mortality associated with population declines in the rain forests of Australia and Central America. *Proc Natl Acad Sci USA* 95:9031–9036.
4. Weldon C, Preez LH, Hyatt AD, Muller R, Speare R (2004) Origin of the amphibian chytrid fungus. *Emerg Infect Dis* 10:2100–2105.
5. Rachowicz LJ, et al. (2006) Emerging infectious disease as a proximate cause of amphibian mass mortality. *Ecology* 87:1671–1683.
6. Nair US, Lawton RO, Welch RM, Pielke RA (2003) Impact of land use on Costa Rican tropical montane cloud forests: Sensitivity of cumulus cloud field characteristics to lowland deforestation. *J Geophys Res* 108:4206.
7. Lawton RO, Nair US, Pielke RA, Welch RM (2001) Climatic impact of tropical lowland deforestation on nearby montane cloud forests. *Science* 294:584–587.
8. Still C, Foster P, Schneider S (1999) Simulating the effects of climate change on tropical montane cloud forests. *Nature* 398:608–610.
9. Pounds JA, Crump ML (1994) Amphibian declines and climate disturbance—the case of the golden toad and the Harlequin frog. *Conservation Biol* 8:72–85.
10. Rohr JR, Raffel TR, Romansic JM, McCallum H, Hudson PJ (2008) Evaluating the links between climate, disease spread, and amphibian declines. *Proc Natl Acad Sci USA* 105:17436–17441.
11. Lips KR, Diffendorfer J, Mendelson JR, III, Sears MW (2008) Riding the wave: Reconciling the roles of disease and climate change in amphibian declines. *PLoS Biol* 6:e72.
12. Evans MN, Schrag DP (2004) A stable isotope-based approach to tropical dendroclimatology. *Geochim Cosmochim Acta* 68:3295–3305.
13. Anchukaitis KJ, Evans MN, Wheelwright NT, Schrag DP (2008) Stable isotope chronology and climate signal in neotropical montane cloud forest trees. *J Geophys Res* 113:G03030.
14. Verheyden A, et al. (2004) Annual cyclicity in high-resolution stable carbon and oxygen isotope ratios in the wood of the mangrove tree *Rhizophora mucronata*. *Plant Cell Environ* 27:1525–1536.
15. Evans MN (2007) Toward forward modeling for paleoclimatic proxy signal calibration: A case study with oxygen isotopic composition of tropical woods. *Geochem Geophy Geosy* 8:Q07008.
16. Evans MN (2008) A reactor for high temperature pyrolysis and oxygen isotopic analysis of cellulose via induction heating. *Rapid Comm Mass Sp* 22:2211–2219.
17. Barbour MM, Roden JS, Farquhar GD, Ehleringer JR (2004) Expressing leaf water and cellulose oxygen isotope ratios as enrichment above source water reveals evidence of a Peclet effect. *Oecologia* 138:426–435.
18. Kaplan A, et al. (1998) Analyses of global sea surface temperature 1856–1991. *J Geophys Res* 103:18567–18589.
19. Kalnay E, et al. (1996) The NCEP/NCAR 40-year reanalysis project. *B Am Meteorol Soc* 77:437–471.
20. Enfield DB, Lee SK, Wang C (2006) How are large Western Hemisphere warm pools formed?. *Prog Oceanogr* 70:346–365.
21. Fleming T (1986) Secular changes in Costa Rican rainfall: Correlation with elevation. *J Trop Ecol* 2:87–91.
22. Peterson TC, Vose RS (1997) An overview of the Global Historical Climatology Network temperature database. *B Am Meteorol Soc* 78:2837–2849.
23. Rhodes AL, Guswa AJ, Newell SE (2006) Seasonal variation in the stable isotopic composition of precipitation in the tropical montane forests of Monteverde, Costa Rica. *Water Resour Res* 42:W11402.
24. Baines PG, Folland CK (2007) Evidence for a rapid global climate shift across the late 1960s. *J Climate* 20:2721–2744.
25. Gu DF, Philander S (1995) Secular changes of annual and interannual variability in the tropics during the past century. *J Climate* 8:864–876.
26. Wang B, Wang Y (1996) Temporal structure of the Southern Oscillation as revealed by waveform and wavelet analysis. *J Climate* 9:1586–1598.
27. Torrence C, Webster PJ (1999) Interdecadal changes in the ENSO–Monsoon System. *J Climate* 12:2679–2690.
28. Mitchell T, Wallace J (1996) ENSO seasonality: 1950–78 versus 1979–92. *J Climate* 9:3149–3161.
29. Giannini A, Cane MA, Kushnir Y (2001) Interdecadal changes in the ENSO teleconnection to the Caribbean region and the North Atlantic oscillation. *J Climate* 14:2867–2879.
30. Veldkamp E, Weitz AM, Staritsky IG, Huising EJ (1992) Deforestation trends in the Atlantic zone of Costa Rica: A case study. *Land Degrad Rehabil* 3:71–84.
31. Allen MR, Robertson AW (1996) Distinguishing modulated oscillations from coloured noise in multivariate datasets. *Clim Dynam* 12:775–784.
32. Allen MR, Smith LA (1996) Monte Carlo SSA: Detecting irregular oscillations in the presence of colored noise. *J Climate* 9:3373–3404.
33. Ghil M, et al. (2002) Advanced spectral methods for climatic time series. *Rev Geophys* 40:1003.
34. Pounds JA, Fogden M, Savage JM, Gorman GC (1997) Tests of null models for amphibian declines on a tropical mountain. *Conservation Biol* 11:1307–1322.
35. Snedecor GW, Cochran WG (1989) *Statistical Methods* (Iowa State Univ Press, Ames, IA), 8th Ed.
36. Enfield DB, Mestas-Nunez AM, Trimble PJ (2001) The Atlantic Multidecadal Oscillation and its relation to rainfall and river flows in the continental US. *Geophys Res Lett* 28:2077–2080.
37. Collins M, and The CMIP Modeling Groups (2005) El Niño—or La Niña-like climate change?. *Clim Dynam* 24:89–104.
38. Latif M, Keenlyside N (2008) El Niño/Southern Oscillation response to global warming. *Proc Natl Acad Sci USA* 10.1073/pnas.0710860105.
39. Rajagopalan B, Lall U, Cane MA (1997) Anomalous ENSO occurrences: An alternate view. *J Climate* 10:2351–2357.
40. Puschendorf R, Bolanos F, Chaves G (2006) The amphibian chytrid fungus along an altitudinal transect before the first reported declines in Costa Rica. *Biol Conserv* 132:136–142.
41. Crump M (2000) *In Search of the Golden Frog* (Univ of Chicago Press, Chicago).
42. Fritts HC (1976) *Tree Rings and Climate* (Academic, New York).
43. McCarroll D, Loader NJ (2004) Stable isotopes in tree rings. *Quaternary Sci Rev* 23:771–801.
44. Lips KR, et al. (2006) Emerging infectious disease and the loss of biodiversity in a Neotropical amphibian community. *Proc Natl Acad Sci USA* 103:3165–3170.
45. Harrison RD (2001) Drought and the consequences of El Niō in Borneo: A case study of figs. *Popul Ecol* 43:63–75.
46. Stapp P, Antolin MF, Ball M (2004) Patterns of extinction in prairie dog metapopulations: Plague outbreaks follow El Nīno events. *Front Ecol Environ* 2:235–240.
47. McMenamin SK, Hadly EA, Wright CK (2008) Climatic change and wetland desiccation cause amphibian decline in Yellowstone National Park. *Proc Natl Acad Sci USA* 105:16988–16993.
48. Burrowes PA, Joglar RL, Green DE (2004) Potential causes for amphibian declines in Puerto Rico. *Herpetologica* 60:141–154.
49. Gould SJ (2002) *I Have Landed* (Harmony, New York), pp 13–15.
50. Brendel O, Iannetta PPM, Stewart D (2000) A rapid and simple method to isolate pure α-cellulose. *Phytochem Analysis* 11:7–10.
51. Anchukaitis KJ, et al. (2008) Consequences of a rapid cellulose extraction technique for oxygen isotope and radiocarbon analyses. *Anal Chem* 80:2035–2041.
52. Bronk Ramsey C, van der Plicht J, Weninger B (2001) "Wiggle matching" radiocarbon dates. *Radiocarbon* 43:381–389.
53. Galimberti M, Bronk Ramsey C, Manning S (2004) Wiggle-match dating of tree-ring sequences. *Radiocarbon* 46:917–924.
54. Robertson I, et al. (2004) The dating of dipterocarp tree rings: Establishing a record of carbon cycling and climatic change in the tropics. *J Quaternary Sci* 19:657–664.
55. Ebisuzaki W (1997) A method to estimate the statistical significance of a correlation when the data are serially correlated. *J Climate* 10:2147–2153.